Published in final edited form as:
Neuron. 2007 April 19; 54(2): 291–301.

Coactivation of Pre- and Postsynaptic Signaling Mechanisms Determines Cell-Specific Spike-Timing-Dependent Plasticity

Thanos Tzounopoulos[1,*], **Maria E. Rubio**[2], **John E. Keen**[1], and **Laurence O. Trussell**[3,4]

1 *Department of Cell Biology and Anatomy, Rosalind Franklin University, Chicago Medical School, North Chicago, IL 60064, USA*

2 *Department of Physiology and Neurobiology, University of Connecticut, Storrs, CT 06269, USA*

3 *Oregon Hearing Research Center, Oregon Health & Science University, Portland, OR 97239, USA*

4 *Vollum Institute, Oregon Health & Science University, Portland, OR 97239, USA*

SUMMARY

Synapses may undergo long-term increases or decreases in synaptic strength dependent on critical differences in the timing between pre- and postsynaptic activity. Such spike-timing-dependent plasticity (STDP) follows rules that govern how patterns of neural activity induce changes in synaptic strength. Synaptic plasticity in the dorsal cochlear nucleus (DCN) follows Hebbian and anti-Hebbian patterns in a cell-specific manner. Here we show that these opposing responses to synaptic activity result from differential expression of two signaling pathways. Ca^{2+}/calmodulin-dependent protein kinase II (CaMKII) signaling underlies Hebbian postsynaptic LTP in principal cells. By contrast, in interneurons, a temporally precise anti-Hebbian synaptic spike-timing rule results from the combined effects of postsynaptic CaMKII–dependent LTP and endocannabinoid-dependent presynaptic LTD. Cell specificity in the circuit arises from selective targeting of presynaptic CB1 receptors in different axonal terminals. Hence, pre- and postsynaptic sites of expression determine both the sign and timing requirements of long-term plasticity in interneurons.

INTRODUCTION

The dorsal cochlear nucleus (DCN) is an auditory brainstem region resembling the cerebellar cortex (Bell, 2002; Oertel and Young, 2004). Its circuitry integrates auditory with somatosensory input and is thought to play a role in the orientation of the head toward sounds of interest (May, 2000; Sutherland et al., 1998; Young and Davis, 2002). However, the mechanism by which the DCN performs its computational tasks remains unclear. The DCN molecular layer consists of excitatory parallel fibers innervating both “cartwheel” interneurons and “fusiform” principal neurons (Mugnaini et al., 1980). Cartwheel cells, in turn, strongly inhibit fusiform cells through feed-forward inhibition (Davis et al., 1996) (Figure 1A).

In studies of long-term synaptic plasticity over the last decade, it has become clear that the direction of change, either strengthening or weakening, can be determined by the precise timing of pre- and postsynaptic action potentials (Bell et al., 1997; Gustafsson et al., 1987; Levy and Steward, 1983; Magee and Johnston, 1997; Markram et al., 1997). This dependence on timing is termed spike-timing-dependent plasticity, or STDP. We have demonstrated unique, opposing forms of STDP at parallel fiber synapses onto fusiform and cartwheel cells (Tzounopoulos et al., 2004). The STDP observed at parallel fiber-fusiform cell synapses resembles STDP observed in the cortex and hippocampus and is Hebbian: presynaptic inputs are strengthened

*Correspondence: athanasios.tzounopoulos@rosalindfranklin.edu.

when they are successful in driving postsynaptic spikes, i.e., LTP is observed when a postsynaptic spike follows the EPSP (Bi and Poo, 1998; Feldman, 2000; Froemke and Dan, 2002; Sjostrom et al., 2001). By contrast, parallel fiber-cartwheel cell synapses are characterized by an anti-Hebbian timing rule: presynaptic inputs that reliably cause, or predict, a postsynaptic spike are weakened, i.e., LTD is observed when a postsynaptic spike follows the EPSP. Similar forms of anti-Hebbian STDP have been observed in the electrosensory system of a weakly electric fish (Bell et al., 1997; Han et al., 2000) and in the cerebellum (Wang et al., 2000). However, in the DCN, the timing requirements for coincident detection of pre- and postsynaptic activity appear more precise when compared to other mammalian synapses exhibiting STDP, particularly with respect to LTD (Dan and Poo, 2006). Computational studies suggest that anti-Hebbian STDP provides a mechanism that equalizes synaptic efficacy along the dendritic tree, thus eliminating location dependence of the synapses (Rumsey and Abbott, 2006). Unlike recent progress on the cellular mechanisms of Hebbian-STDP (Bender et al., 2006; Dan and Poo, 2006; Sjostrom et al., 2003; Nevian and Sakmann, 2006), the mechanisms underlying anti-Hebbian STDP remain unclear.

We have examined signaling mechanisms underlying STDP in the DCN and found that anti-Hebbian LTD in cartwheel cells is mediated by retrograde endocannabinoid signaling. However, the timing rule that results from this signaling is opposed by the presence of a postsynaptic CaMKII-dependent mechanism that acts to strengthen synaptic communication. Excitatory synapses onto principal cells lack the endocannabinoid system and thus only express a Hebbian LTP. Specifically, electrophysiological and electron-microscopic data suggest that endocannabinoid signaling is less prominent in fusiform cells as a result of differential distribution of endocannabinoid receptors on terminals of single axons. Thus, a decrease in transmitter release mediated by endocannabinoids and increase in transmitter sensitivity mediated by CaMKII signaling together shape the spike-timing rule in a synapse-specific manner.

RESULTS

Anti-Hebbian LTD Is Induced Postsynaptically but Expressed Presynaptically

We investigated the underlying induction and expression mechanisms of anti-Hebbian LTD in cartwheel cells using pharmacological tools. LTD was induced using a conditioning protocol in which a postsynaptic spike was triggered 5 ms after the onset of a parallel-fiber-evoked EPSP, as shown previously (Tzounopoulos, et al., 2004). The N-methyl-D-aspartate receptor (NMDAR) antagonists DL-2-amino-5-phosphonovalerate (APV, 100 μM applied to the bath) or MK-801 (20 μM, applied intracellularly) blocked LTD, as did intracellular application of 1,2-bis (o-aminophenoxy)ethane-N,N,N′,N′-tetraacetic acid (BAPTA, 20 mM, Figure 1B). Therefore, the induction of LTD requires a postsynaptic rise in Ca^{2+}, probably mediated by postsynaptic NMDARs. To investigate expression mechanisms, we used two assays that are sensitive to changes in neurotransmitter release: paired-pulse facilitation (PPF; Zucker and Regehr, 2002) and coefficient of variation (CV) analysis (Faber and Korn, 1991; Larkman et al., 1992; Tsien and Malinow, 1991). PPF was increased after LTD induction, suggesting a decrease in probability of release associated with LTD expression (Figure 1C). Induction of LTD was paralleled by a reduction in $1/CV^2$; a similar reduction was seen with baclofen, which is known to inhibit the postsynaptic response via a presynaptic mechanism (Figure 1D). By contrast, 0.5 μM 6,7-dinitroquinoxaline-2, 3-dione (DNQX), which reduces responses by partially blocking postsynaptic glutamate receptors, left CV and paired-pulse plasticity unaffected (Figures 1C and 1D). We conclude that anti-Hebbian LTD is induced postsynaptically, but expressed presynaptically.

Endocannabinoid Signaling Underlies LTD and Masks LTP

Given the role of endocannabinoids in retrograde signaling in the cerebellar cortex, and the strong parallels between Purkinje neurons and cartwheel cells (Berrebi and Mugnaini, 1988; Manis et al., 1994; Wouterlood and Mugnaini, 1984; Zhang and Oertel, 1993), we tested whether endocannabinoid signaling is involved in LTD in the cartwheel cell. Endocannabinoids are released from postsynaptic cells and diffuse to presynaptic terminals where they activate endocannabinoid (CB1) receptors (Freund et al., 2003; Piomelli et al., 1998; Wilson and Nicoll, 2002). CB1 receptors are G protein-coupled receptors that inhibit transmitter release (Hajos et al., 2001; Hoffman and Lupica, 2000; Kreitzer and Regehr, 2001a; Ohno-Shosaku et al., 2001; Wilson and Nicoll, 2001). Endocannabinoid signaling has been previously shown to mediate Hebbian LTD in different brain regions (Auclair et al., 2000; Bender et al., 2006; Chevaleyre and Castillo, 2003; Gerdeman et al., 2002; Huang et al., 2003; Marsicano et al., 2002; Robbe et al., 2002; Safo and Regehr, 2005; Sjostrom et al., 2003). Using an induction protocol wherein the EPSP preceded the spike by 4–5 ms, application of 1 μM AM-251 (a selective CB1 receptor antagonist) not only blocked LTD but, surprisingly, also unmasked a long-term potentiation (Figure 2A). AM-251 had no effect on baseline synaptic transmission (see Figure S1 in the Supplemental Data available online), indicating lack of tonic activation of CB1 receptors. Given the involvement of group I metabotropic glutamate receptors (mGluRs) in endocannabinoid-mediated LTD in other systems (Chevaleyre and Castillo, 2003), we tested the role of mGluR1 and -5 on the induction of LTD. Bath application of 100 μM LY367385 and 4 μM MPEP, selective antagonists of mGluR subtypes 1 and 5, respectively, had no effect on cartwheel cell LTD (Figure 2C), indicating that mGluR1/5 activation is not necessary for LTD induction. Next we determined the induction and expression mechanisms of the "unmasked" LTP. Application of extracellular APV or intracellular BAPTA was able to block this form of LTP, suggesting that both signaling cascades leading to LTP and LTD are initiated in the postsynaptic cell by a rise in Ca^{2+}, probably mediated by NMDARs (Figure 2B). As with LTP in hippocampal pyramidal neurons (Malenka and Nicoll, 1999), this "unmasked" LTP was mediated through a postsynaptic mechanism because, PPF and $1/CV^2$ did not change after its induction (Figures 2D and 2E) and LTP was blocked by intracellularly applied CaMKII peptide inhibitor (Chang et al., 2001; Yasuda et al., 2003) (CaMKII-Ntide, 10–50 μM) (Figure 2B).

Coincidence Detection Windows for Anti-Hebbian LTD and Hebbian LTP

To determine the relative roles of these signaling pathways in shaping the dependence of plasticity on timing, we applied selective blockers of each of the two pathways and monitored the change in EPSP amplitude after conditioning trains with different EPSP spike-timing relationships. CaMKII-Ntide, applied through the recording pipette, was used to block CaMKII signaling and thus permitted us to study the learning rule determined by endocannabinoid signaling, while AM-251 was used to block endocannabinoid signaling. The black squares in Figure 3A are control data showing that LTD is only observed for an EPSP spike-timing delay of 4–5 ms (Tzounopoulos et al., 2004). When endocannabinoid signaling was blocked with AM-251, the timing curve (triangles, Figure 3A) revealed LTP that was triggered between 5 and 20 ms pre-post pairing protocol. Thus, both the polarity and the timing sensitivity had changed. Interestingly, this broader timing window is similar to that observed for timing-dependent LTP in fusiform cells (Tzounopoulos et al., 2004). When CaMKII signaling was blocked with CaMKII-Ntide, the observed timing rule was anti-Hebbian, but the timing window for coincident detection increased, a mirror-image of the relationship seen in AM-251 (circles, Figure 3A). At a 10 ms delay, no plasticity is seen in controls, and this appears to reflect the cancelling of the effects of presynaptic endocannabinoid-mediated LTD and postsynaptic CaMKII-mediated LTP occurring simultaneously. When the spike follows the EPSP by only 5 ms, additional LTD is observed after blocking LTP (Figure 3A). Since peptide diffusion from the patch pipette into dendritic spines may be limited, we tried a higher peptide

concentration (200 μM), which produced a weak potentiating effect on baseline EPSP amplitude but also revealed an even stronger LTD when tested at the 5 ms EPSP spike interval (Figure S2). At either zero or −5 ms, no plasticity was observed under any recording condition (Figure 3A). These results show that the unique, narrow timing plot rule for the interneuron reflects the interaction of distinct metabolic pathways and plasticities expressed on both sides of the synapse.

The polarity of synaptic plasticity in cartwheel cells is frequency dependent (Tzounopoulos et al., 2004). Anti-Hebbian LTD was observed at low frequencies (10 Hz; Figures 3A and 3B), while LTP was induced at 40 Hz, regardless of the timing order of pre- and postsynaptic activity (Tzounopoulos et al., 2004) (Figure 3B). When AM-251 was applied, the LTP was not significantly different at 10 Hz or 40 Hz, nor was it different from the LTP seen at 40 Hz in control conditions (Figure 3B). Therefore, LTP observed at 40 Hz in control conditions is mediated by CaMKII signaling and its effects apparently dominate over endocannabinoid signaling. After blocking CaMKII signaling, a larger-magnitude LTD could be induced at 10 Hz (Figure 3B). Thus, learning rules are not static, but depend both on the frequency of synaptic activity and on the relative timing of pre- and postsynaptic activity.

Cell-Specific Expression of Endocannabinoid Signaling Determines the Type of Associative Plasticity

Parallel fibers are known to contact both cartwheel and fusiform cells, yet these cells exhibit strikingly different timing plots in STDP paradigms (Tzounopoulos et al., 2004). Could the differential distribution of the signaling mechanisms described above account for cell-specific synaptic learning rules? In fusiform cells, which do not exhibit anti-Hebbian plasticity, blockade of either NMDAR or CaMKII prevented induction of LTP (Figure 4A). Additionally, PPF and CV did not change after its induction, indicating a postsynaptic site of LTP expression (Figures 4B and 4C), similar to that of cartwheel cells. These results suggest that selective engagement of endocannabinoid signaling in cartwheel cells and its interaction with the CaMKII signaling cascade may explain site-specific STDP in the DCN. If the plasticity in cartwheel cells is different from that observed in fusiform cells solely because of engagement of endocannabinoid signaling, then we would predict that parallel fiber terminals innervating fusiform cells do not express CB1 receptors and/or that fusiform cells do not release endocannabinoids, at least under the induction protocol used in this study.

To distinguish between these two possibilities, we used physiological and histological approaches. Depolarization-induced suppression of excitation (DSE) is a transient decrease in synaptic strength of excitatory inputs that is mediated by endocannabinoids (Kreitzer and Regehr, 2001b) and was used here to reveal endocannabinoid signaling in cartwheel and fusiform cells. Application of 1 s depolarization to 0 mV in cartwheel cells led to a decrease of synaptic strength that lasted ~10–15 s (Figure 5A). This decrease was mediated by endocannabinoids, as application of AM-251 was able to block this decrease (Figure 5C). DSE in fusiform cells was much smaller than in cartwheel cells (Figures 5A–5C). We then asked how sensitive parallel fiber synapses on the two cell types are to an agonist of CB1 receptor. When WIN-55,212-2 (1 μM), was bath applied, a quantitatively similar decrease of synaptic strength was observed both in cartwheel and fusiform cells (Figures 5D and 5F); however, the onset of block of synapses on fusiform cells was distinctly slower. This difference was not due to differential penetration of the drug, as we were careful not to record from fusiform cells located in deeper layers of the slice. When the concentration of WIN-55,212-2 was reduced to 50 nM (Figures 5E and 5F), a more gradual and limited block of transmission at cartwheel synapses was seen, and almost no effect was observed in fusiform cells, after 35 min of incubation. These data suggest that parallel fiber terminals may differ in their density of CB1 receptors.

This interpretation was confirmed through EM immunolocalization of CB1 receptors (Figure 6). Postembedding immunolocalization was performed using antibodies directed against either the entire C terminus (Figure 6) or a 15 amino acid section of the protein (Figure S3) of the CB1 receptors, with comparable results. Five-nanometer gold particles were apparent within parallel fiber terminals onto both cell types (Figures 6A–6F) and on the spines of cartwheel cells (Figures 6A–6C). The distribution of presynaptic particles was quantified as shown in the cartoon in Figure 6G; particles were classified as being associated with membrane facing the postsynaptic density (PSD), at the periphery of the PSD, or in extrasynaptic membrane areas. Particles had to be within 40 nm of presynaptic plasma membrane to qualify as membrane labeling (see Experimental Procedures). With these criteria, a striking difference in distribution was apparent, such that parallel fiber-cartwheel synapses had more membrane labeling than synapses onto fusiform cells, and most of that labeling was facing the PSD (Figure 6G). Intraterminal labeling was not different between the two classes of terminal (Figure 6H). Thus, these data confirm that differential endocannabinoid signaling may be caused by cell-selective expression of CB1 receptors at terminals of parallel fibers.

DISCUSSION

By using electrophysiological and anatomical techniques, we revealed mechanisms underlying cell-specific STDP in the DCN. Our findings show that differences in cell-specific synaptic learning rules can be ascribed to differences in the subcellular targeting of presynaptic endocannabinoid receptors. We also show that the uniquely narrow timing windows for STDP observed in the DCN represent the convergent effects of presynaptic endocannabinoid signaling and postsynaptic CaMKII signaling. The convergence and modulation of different signaling pathways to modify synaptic strength adds a new layer of intricacy and flexibility to neuronal networks.

Cellular Mechanisms Underlying STDP

Two general mechanisms are thought to underlie Hebbian STDP. In one, postsynaptic NMDARs represent the main coincidence detector for STDP (Froemke et al., 2005; Nishiyama et al., 2000; Shouval et al., 2002). Similar to LTP and LTD induced by conventional protocols, in STDP, pre-post spiking (EPSP followed by spike) leads to brief high-level Ca^{2+} influx due to effective activation of NMDARs (LTP pathway), while post-pre spiking (spike followed by EPSP) leads to a low-level Ca^{2+} rise (LTD pathway). Ca^{2+} imaging studies have demonstrated supralinear summation with pre-post spiking and sublinear summation with post-pre spiking (Koester and Sakmann, 1998; Nevian and Sakmann, 2004). However, such a simple model seems unlikely to provide sufficient explanation for the whole STDP window. This model predicts the existence of an LTD window at positive (pre-post) intervals longer than those for LTP induction. At this interval, the gradual decrease of Ca^{2+} through NMDARs must reach a range appropriate for LTD induction before coming back to baseline levels. Such a broader window has not been consistently observed (but see Nishiyama et al., 2000). A second mechanism was hypothesized by Karmarkar and Buonomano (2002), in which a second coincident detector independent of NMDARs is proposed for explaining LTD observed at post-pre intervals. This second scheme recently found experimental support (Bender et al., 2006; Nevian and Sakmann, 2006) and involves separate Ca^{2+} sources and coincident detection for LTP and LTD. LTP shows classical NMDAR dependence. LTD was independent of NMDARs and involved mGLURs, Ca^{2+} from voltage-sensitive channels, and IP_3 receptor-gated stores from the postsynaptic cell. This sequence of events triggers retrograde endocannabinoid signaling as well as activation of presynaptic NMDARs, leading to presynaptic LTD.

Here we explored the cellular mechanisms underlying anti-Hebbian STDP. We discovered that for pre-post pairs, both LTD and LTP observed in cartwheel cells use NMDARs as the

coincidence detector. Conventional CaMKII signaling mediates Hebbian LTP. Endocannabinoids were first shown to mediate Hebbian spike-timing-dependent LTD in the neocortex (Sjostrom et al., 2003). In that study, LTD required simultaneous activation of presynaptic NMDA and CB1 receptors. We find that retrograde endocannabinoid signaling, recently shown to be involved in some other forms of Hebbian LTD (Bender et al., 2006), can also mediate anti-Hebbian LTD. Most strikingly, we find that these distinct signaling pathways occur simultaneously and thus together determine the sign of the observed plasticity and shape the timing window. At the various pre-post intervals tested, the EPSP reflects the product of changes in quantal release and quantal size triggered by endocannabinoid and CaMKII pathways, respectively. For example, at the 5 ms interval, a peak LTP in the presence of AM-251 was 152% of prestimulus control. At the same interval in CaMKII-Ntide, the EPSP was 61% in 10–50 μM peptide (Figure 3A) and 50% with 200 μM peptide (Figure S2), which we assume is a maximal response. The product of the effects on release and sensitivity (1.52 × 0.5) gives an EPSP of 76% of control, similar to our value of 74% in the absence of inhibitors (Figure 3A). Remarkably, the effects of the inhibitors suggest that, at time points like +10 ms in which no change in EPSP size is induced, pre- and postsynaptic plasticity have produced effects that exactly cancel one another.

These proposed mechanisms differ from a recent study in cortex that revealed anti-Hebbian LTD at distal dendritic inputs while the same stimulus induced Hebbian LTP at proximal dendrites (Sjostrom and Hausser, 2006). Anti-Hebbian LTD in that study was the result of limited spread of backpropagating action potentials at distal synapses, which created a gradient of LTP and LTD as the distance between synaptic contacts and the soma increased. Recent reports suggest that synaptic plasticity results from the balance between separately activated induction pathways for LTP and LTD (Bender et al., 2006; Liu et al., 2004; O'Connor et al., 2005; Wang et al., 2005; Wittenberg and Wang, 2006). In these cases, linear summation of LTP and LTD components determine the overall associative plasticity rule. Our results differ in that we find that LTP and LTD mechanisms have different sites of action (pre-versus postsynaptic) yet occur simultaneously. Such simultaneous LTP and LTD was also suggested recently by Sjostrom et al. (2007); there, existing LTP was enhanced by blocking CB1 receptors, suggesting that an LTD tempered the magnitude of LTP.

Our results also reveal that the relative dominance of signaling pathways is frequency dependent (Figure 3B). At the higher stimulus frequency, LTP observed with high-frequency stimuli is mediated by CaMKII signaling and dominates over endocannabinoid signaling. Given the prominent role of Ca^{2+} and the presence of heavily spine-laden dendrites in cartwheel cells, local, rapid changes in Ca^{2+} could determine signaling pathway dominance. Since some forms of plasticity in cartwheels cells also depend on intracellular store Ca^{2+} (Fujino and Oertel, 2003), the activation or inhibition of Ca^{2+}-induced Ca^{2+} release channels may also participate in this process (Bender et al., 2006; Wang et al., 2000). Regardless of the mechanism for STDP induction, it is clear that the frequency dependence of different signaling mechanisms in shaping synaptic learning rules provide a new way of modifying the rules for associative plasticity. These mechanisms not only may allow for a single cell type to change its synaptic coding rules in an activity-dependent manner but also permit networks to create population-specific learning rules.

Cell-Specific Expression of Endocannabinoid Signaling Determines Cell-Specific Synaptic Plasticity

Cell-specific short- and long-term plasticities have been previously observed in different neural circuits. Target cells may determine the probability of release and short-term plasticity of synapses, thus allowing for the same fibers to influence their targets differentially (Markram et al., 1998; Pouille and Scanziani, 2004; Reyes et al., 1998; Rozov et al., 2001; Thomson,

1997; Toth et al., 2000). To our knowledge, our findings reveal a novel mechanism for cell-specific modulation of Hebbian and anti-Hebbian STDP by endocannabinoids which depends on the terminal-specific targeting of presynaptic CB1 receptors (Figure S4). While application of an agonist of the CB1 receptor inhibited transmission at both cell types, the extent of inhibition was different when submaximal doses were used. The differential distribution of the receptors on parallel fiber terminals, perhaps their relative distance to Ca^{2+} channels, might account for the difference in agonist effectiveness, as supported by ultrastuctural analysis. Although not excluding the possibility of difference in endocannabinoid release between the two cell types, these results show that similar effectiveness of high concentrations of agonist cannot be taken as evidence for differential endocannabinoid release. The ability of the various terminals to selectively target receptors according to the postsynaptic cell type has been observed in other systems (Toth et al., 2000) but here takes on the role of dictating the polarity of long-term plasticity within a synaptically coupled network. The functional significance of cell-specific engagement of endocannabinoid signaling may be to tune the effect of feed-forward inhibition to the fusiform cells. Cartwheel cells form a powerful interneuronal network that shuts off fusiform cell firing (Davis et al., 1996). Preferential DSE of parallel fiber inputs to cartwheel cells may gate initiation of activity to fusiform cells, which are heavily inhibited in vivo in response to parallel fiber stimulation (Davis et al., 1996). In addition, cell-specific STDP synergistically increases excitability of the output neuron by potentiating the excitatory input to the fusiform cells while at the same time reducing the inhibitory input to fusiform cells. However, this balance is shifted at 40 Hz, where increased parallel fiber activity leads to LTP in parallel fiber inputs to cartwheel cells. This would result in increased feed-forward inhibition, thus preventing runaway excitation of fusiform cells.

Functional Role of Anti-Hebbian STDP in the DCN

What are the roles of adaptive synaptic learning rules for the computational tasks performed by the DCN? Similarities to cerebellum-like structures in the fish and to the cerebellum itself may provide clues as to the significance of adaptive synaptic learning rules and multimodal integration. In cerebellum-like sensory structures in electric fish, anti-Hebbian parallel fiber synaptic plasticity serves to cancel out the predictable sensory consequences of the fish's own motor actions (Bell, 1981; Bell et al., 1997; Roberts and Bell, 2000). Anti-Hebbian STDP observed in cartwheel cells may underlie a similar adaptive filtering role in the DCN. Information about the position of the head and neck relayed by parallel fibers provides the "raw material" that would be needed to cancel predictable consequences of movements on auditory input. Also, such plasticity may aid in responding to novel sounds by suppressing the response to self-generated or expected sounds. A detailed conceptual model of how such schemes might be implemented in the DCN has yet to emerge. However, our data support the idea that the computational tasks of the DCN may be changing according to activity levels or the availability of different metabolic pathways. Therefore, Hebbian synaptic learning rules induced during increased activity or modulation of endocannabinoid or CaMKII signaling may transform the computational tasks of the DCN. Instead of creating a "negative image" of ongoing activity, Hebbian synaptic learning rules may create a memory trace (Yao and Dan, 2001) that sensitizes the DCN to particular profiles of subsequent auditory and nonauditory stimuli.

EXPERIMENTAL PROCEDURES

Electrophysiology

Coronal brain slices were made from ICR mice (P18–P25). Animals were sacrificed according to methods approved by the Institutional Animal Care and Use Committee of OHSU and the Rosalind Franklin University. Single cells were visualized with IR interference contrast optics and recorded using patch pipettes in either voltage- or current-clamp modes. Cells in the DCN's fusiform cell layer were identified on the basis of morphological and electrophysiological

criteria (Tzounopoulos et al., 2004). The external solution contained (in mM) 130 NaCl, 3 KCl, 1.2 KH_2PO_4, 2.4 $CaCl_2$, 1.3 $MgSO_4$, 20 $NaHCO_3$, 3 HEPES, and 10 glucose; saturated with 95% O_2/5% CO_2. Pipettes were filled with a K-based solution, containing (in mM) 113 K-gluconate, 4.5 $MgCl_2$, 14 trisphosphocreatine, 9 HEPES, 0.1 EGTA, 4 Na-ATP, 0.3 tris-GTP at pH 7.3. Fiber tracts were stimulated with voltage pulses (100 μs, 7–30 V). All experiments were performed at room temperature. Input resistance was monitored from a response to a hyperpolarizing step during each sweep. Experiments were not included if the input resistance changed more than 20% over 50–60 min. Stimulus intensity was set to evoke subthreshold, single-component EPSPs. Action potentials were evoked by somatic current injection. For voltage-clamp experiments, series resistance was monitored throughout the experiment from the size and shape of the capacitive transient in response to a 5 mV hyperpolarization, after compensation of pipette capacitance. Input resistance was calculated from the sustained response to the same step. EPSC amplitude was defined as the mean amplitude during a 1–2 ms window at the peak of the EPSC minus the amplitude during a similar window immediately before the stimulus artifact.

Mean, baseline, EPSP slope, or amplitude was calculated from 50–100 sweeps immediately before the start of pairing. Postpairing slope or amplitude was calculated from 20–30 min after the end of pairing. EPSCs were used for CV analysis. CV was corrected for the background noise, and mean and $1/CV^2$ were normalized to the control value. All means are reported ± SEM. Statistical comparisons were made using unpaired two-tailed Student's t tests of average EPSPs before pairing with a mean of EPSPs during a 7–10 min window taken 20 min after pairing. Statistical significance was based on p values < 0.05. Nonsignificant comparisons are indicated as ns.

Tissue Preparation for Electron Microscopy

The handling and care of the animals prior to and during the experimental procedures were approved and supervised by the University of Connecticut IACUC and followed NIH guidelines. For structural analysis, 2 postnatal day 22 CD-1 mice were used. Mice were anesthetized with a mixture of ketamine 60 mg/kg and xylazine 6.5 mg/kg. After checking anesthetic depth, mice were perfused with 4% paraformaldehyde and 0.5% glutaraldehyde in 0.12 M phosphate buffer (pH 7.2) for 10 min. Low glutaraldehyde fixation was then followed by cryofixation and freeze-substitution as previously described (Matsui et al., 2005).

Postembedding Immunogold Labeling Procedure after Freeze-Substitution

Two well-characterized, affinity-purified polyclonal antibodies against the carboxyl terminus of the CB1 receptor subunit (CT and L15; Nyíri et al., 2005; kindly provided by Dr. K. Mackie, University of Washington) were used at a dilution of 1:200 and labeled with 5 nm colloidal gold-coupled secondary antibodies (Amersham, Piscataway). The CT antibody was raised against the GST fusion protein containing the last 72 amino acids of rat CB1. The L15 antibody was raised against a GST fusion protein containing the last 15 amino acids of rat CB1. The two antibodies showed the same staining pattern in post-embedding immunogold labeling. The data presented in Figure 6 correspond to the analysis performed with the CT antibody. Controls included omitting the primary antibody and preadsorption of primary antibody with the corresponding blocking protein. Electron micrographs were taken at 34,300× magnification with a Philips 300M TEM and scanned at a resolution of 1,600 dpi using an Epson Expression 1680 scanner. Immunostaining was also analyzed with a TECNAI 12 Biotwin TEM. The images were captured with an AMT CCD camera at 49,000× magnification. Image processing was performed with Adobe Photoshop by using only the brightness and contrast commands to enhance gold particles.

Identification of Parallel Fiber Synapses on Fusiform and Cartwheel Cell in the DCN at the Transmission Electron Microscopy Level

EM identification of parallel fiber synapses on fusiform cells was based on the following well-established criteria (Mugnaini, 1985; Rubio and Juiz, 2004): (1) their location in the molecular layer of the DCN (parallel fibers are described as unmyelinated axons that run parallel to the surface of the nucleus) and (2) their ultrastructural characteristics. The parallel fiber synapses are small synaptic endings, which contain small, clear synaptic vesicles and make asymmetrical synaptic contacts (Gray I) onto spines and/or dendritic shafts of apical dendrites of fusiform cells. Parallel fiber synapses on dendritic spines of cartwheel cells were identified based on published criteria (Berrebi and Mugnaini, 1991; Rubio and Juiz, 2004; Wouterlood and Mugnaini, 1984). Location in the nucleus was also used to identify cell bodies and dendrites. Cartwheel cell bodies were located between the fusiform and molecular layer, and most of the dendritic spines analyzed were located in the most apical 100 μm of the DCN (this measurement was estimated based on grid-hole width). Dendritic spines of cartwheel cells are abundant in the molecular layer and are easily recognized because they are large, have an elliptical shape, and are enriched with membranes of smooth endoplasmic reticulum.

Quantitative Evaluation of CB1 Receptor Immunolabeling at Parallel Fiber Synaptic Endings on Cartwheel and Fusiform Cells

The distribution and relative density of the CB1 receptor subunit immunolabeling in the parallel fiber synaptic endings on cartwheel and on fusiform cells were determined for 120 synapses (parallel fiber/cartwheel cell = 70 and parallel fiber/fusiform cell = 50). A total of 500 gold particles labeling CB1 receptor were counted. The distance between the center of each gold particle and the outer leaflet of the parallel fiber plasma membrane facing and not facing the PSD of cartwheel and on fusiform cells was measured. The linear density of gold particles at the parallel fiber plasma membrane facing the PSD, facing the periphery of the PSD, and the extrasynaptic plasma membrane (Figure 6) was computed with NIH JScion Image by dividing the number of gold particles at those membrane regions by the length of that profile. The density of intracellular labeling in the parallel fiber synaptic ending was calculated by dividing the number of gold particles in a profile by the area of that profile. The average linear density and density per area were computed across all profiles. Two-tailed t tests (assuming unequal variance) and ANOVA were used for statistical comparison.

Supplementary Material

Refer to Web version on PubMed Central for supplementary material.

Acknowledgements

We thank Drs. Curtis Bell, Matthew Frerking, and Anastassios Tzingounis for critical and helpful comments; Dr. Ken Mackie for providing antibodies; and Drs. Thomas Soderling and Gary Wayman for providing CaMKII peptide-inhibitor. This work was supported by startup funds to T.T. from Rosalind Franklin University and from NIH grants: R37NS28901 to L.O.T., RO1 DC006881-01A2 to M.E.R., and R01 DC007905-01A1 to T.T.

References

Auclair N, Otani S, Soubrie P, Crepel F. Cannabinoids modulate synaptic strength and plasticity at glutamatergic synapses of rat prefrontal cortex pyramidal neurons. J Neurophysiol 2000;83:3287–3293. [PubMed: 10848548]

Bell CC. An efference copy which is modified by reafferent input. Science 1981;214:450–453. [PubMed: 7291985]

Bell CC. Evolution of cerebellum-like structures. Brain Behav Evol 2002;59:312–326. [PubMed: 12207086]

Bell CC, Han VZ, Sugawara Y, Grant K. Synaptic plasticity in a cerebellum-like structure depends on temporal order. Nature 1997;387:278–281. [PubMed: 9153391]

Bender VA, Bender KJ, Brasier DJ, Feldman DE. Two coincidence detectors for spike timing-dependent plasticity in somatosensory cortex. J Neurosci 2006;26:4166–4177. [PubMed: 16624937]

Berrebi AS, Mugnaini E. Effects of the murine mutation 'nervous' on neurons in cerebellum and dorsal cochlear nucleus. J Neurocytol 1988;17:465–484. [PubMed: 3193127]

Berrebi AS, Mugnaini E. Distribution and targets of the cartwheel cell axon in the dorsal cochlear nucleus of the guinea pig. Anat Embryol (Berl) 1991;183:427–454. [PubMed: 1862946]

Bi GQ, Poo MM. Synaptic modifications in cultured hippocampal neurons: dependence on spike timing, synaptic strength, and postsynaptic cell type. J Neurosci 1998;18:10464–10472. [PubMed: 9852584]

Chang BH, Mukherji S, Soderling TR. Calcium/calmodulin-dependent protein kinase II inhibitor protein: localization of isoforms in rat brain. Neuroscience 2001;102:767–777. [PubMed: 11182241]

Chevaleyre V, Castillo PE. Heterosynaptic LTD of hippocampal GABAergic synapses: a novel role of endocannabinoids in regulating excitability. Neuron 2003;38:461–472. [PubMed: 12741992]

Dan Y, Poo MM. Spike timing-dependent plasticity: from synapse to perception. Physiol Rev 2006;86:1033–1048. [PubMed: 16816145]

Davis KA, Miller RL, Young ED. Effects of somatosensory and parallel-fiber stimulation on neurons in dorsal cochlear nucleus. J Neurophysiol 1996;76:3012–3024. [PubMed: 8930251]

Faber DS, Korn H. Applicability of the coefficient of variation method for analyzing synaptic plasticity. Biophys J 1991;60:1288–1294. [PubMed: 1684726]

Feldman DE. Timing-based LTP and LTD at vertical inputs to layer II/III pyramidal cells in rat barrel cortex. Neuron 2000;27:45–56. [PubMed: 10939330]

Freund TF, Katona I, Piomelli D. Role of endogenous cannabinoids in synaptic signaling. Physiol Rev 2003;83:1017–1066. [PubMed: 12843414]

Froemke RC, Dan Y. Spike-timing-dependent synaptic modification induced by natural spike trains. Nature 2002;416:433–438. [PubMed: 11919633]

Froemke RC, Poo MM, Dan Y. Spike-timing-dependent synaptic plasticity depends on dendritic location. Nature 2005;434:221–225. [PubMed: 15759002]

Fujino K, Oertel D. Bidirectional synaptic plasticity in the cerebellum-like mammalian dorsal cochlear nucleus. Proc Natl Acad Sci USA 2003;100:265–270. [PubMed: 12486245]

Gerdeman GL, Ronesi J, Lovinger DM. Postsynaptic endocannabinoid release is critical to long-term depression in the striatum. Nat Neurosci 2002;5:446–451. [PubMed: 11976704]

Gustafsson B, Wigstrom H, Abraham WC, Huang YY. Long-term potentiation in the hippocampus using depolarizing current pulses as the conditioning stimulus to single volley synaptic potentials. J Neurosci 1987;7:774–780. [PubMed: 2881989]

Hajos N, Ledent C, Freund TF. Novel cannabinoid-sensitive receptor mediates inhibition of glutamatergic synaptic transmission in the hippocampus. Neuroscience 2001;106:1–4. [PubMed: 11564411]

Han VZ, Grant K, Bell CC. Reversible associative depression and nonassociative potentiation at a parallel fiber synapse. Neuron 2000;27:611–622. [PubMed: 11055442]

Hoffman AF, Lupica CR. Mechanisms of cannabinoid inhibition of GABA(A) synaptic transmission in the hippocampus. J Neurosci 2000;20:2470–2479. [PubMed: 10729327]

Huang YC, Wang SJ, Chiou LC, Gean PW. Mediation of amphetamine-induced long-term depression of synaptic transmission by CB1 cannabinoid receptors in the rat amygdala. J Neurosci 2003;23:10311–10320. [PubMed: 14614090]

Karmarkar UR, Buonomano DV. A model of spike-timing dependent plasticity: one or two coincidence detectors? J Neurophysiol 2002;88:507–513. [PubMed: 12091572]

Koester HJ, Sakmann B. Calcium dynamics in single spines during coincident pre- and postsynaptic activity depend on relative timing of back-propagating action potentials and subthreshold excitatory postsynaptic potentials. Proc Natl Acad Sci USA 1998;95:9596–9601. [PubMed: 9689126]

Kreitzer AC, Regehr WG. Cerebellar depolarization-induced suppression of inhibition is mediated by endogenous cannabinoids. J Neurosci 2001a;21:RC174. [PubMed: 11588204]

Kreitzer AC, Regehr WG. Retrograde inhibition of presynaptic calcium influx by endogenous cannabinoids at excitatory synapses onto Purkinje cells. Neuron 2001b;29:717–727. [PubMed: 11301030]

Larkman A, Hannay T, Stratford K, Jack J. Presynaptic release probability influences the locus of long-term potentiation. Nature 1992;360:70–73. [PubMed: 1331808]

Levy WB, Steward O. Temporal contiguity requirements for long-term associative potentiation/depression in the hippocampus. Neuroscience 1983;8:791–797. [PubMed: 6306504]

Liu L, Wong TP, Pozza MF, Lingenhoehl K, Wang Y, Sheng M, Auberson YP, Wang YT. Role of NMDA receptor subtypes in governing the direction of hippocampal synaptic plasticity. Science 2004;304:1021–1024. [PubMed: 15143284]

Magee JC, Johnston D. A synaptically controlled, associative signal for Hebbian plasticity in hippocampal neurons. Science 1997;275:209–213. [PubMed: 8985013]

Malenka RC, Nicoll RA. Long-term potentiation—a decade of progress? Science 1999;285:1870–1874. [PubMed: 10489359]

Manis PB, Spirou GA, Wright DD, Paydar S, Ryugo DK. Physiology and morphology of complex spiking neurons in the guinea pig dorsal cochlear nucleus. J Comp Neurol 1994;348:261–276. [PubMed: 7814691]

Markram H, Lubke J, Frotscher M, Sakmann B. Regulation of synaptic efficacy by coincidence of postsynaptic APs and EPSPs. Science 1997;275:213–215. [PubMed: 8985014]

Markram H, Wang Y, Tsodyks M. Differential signaling via the same axon of neocortical pyramidal neurons. Proc Natl Acad Sci USA 1998;95:5323–5328. [PubMed: 9560274]

Marsicano G, Wotjak CT, Azad SC, Bisogno T, Rammes G, Cascio MG, Hermann H, Tang J, Hofmann C, Zieglgansberger W, et al. The endogenous cannabinoid system controls extinction of aversive memories. Nature 2002;418:530–534. [PubMed: 12152079]

Matsui K, Jahr CE, Rubio ME. High-concentration rapid transients of glutamate mediate neural-glial communication via ectopic release. J Neurosci 2005;25:7538–7547. [PubMed: 16107641]

May BJ. Role of the dorsal cochlear nucleus in the sound localization behavior of cats. Hear Res 2000;148:74–87. [PubMed: 10978826]

Mugnaini E. GABA neurons in the superficial layers of the rat dorsal cochlear nucleus: light and electron microscopic immunocytochemistry. J Comp Neurol 1985;235:61–81. [PubMed: 3886718]

Mugnaini E, Warr WB, Osen KK. Distribution and light microscopic features of granule cells in the cochlear nuclei of cat, rat, and mouse. J Comp Neurol 1980;191:581–606. [PubMed: 6158528]

Nevian T, Sakmann B. Single spine Ca2+ signals evoked by coincident EPSPs and backpropagating action potentials in spiny stellate cells of layer 4 in the juvenile rat somatosensory barrel cortex. J Neurosci 2004;24:1689–1699. [PubMed: 14973235]

Nevian T, Sakmann B. Spine Ca2+ signaling in spike-timing-dependent plasticity. J Neurosci 2006;26:11001–11013. [PubMed: 17065442]

Nishiyama M, Hong K, Mikoshiba K, Poo MM, Kato K. Calcium stores regulate the polarity and input specificity of synaptic modification. Nature 2000;408:584–588. [PubMed: 11117745]

Nyíri G, Cserep C, Szabadits E, Mackie K, Freund TF. CB1 cannabinoid receptors are enriched in the perisynaptic annulus and on preterminal segments of hippocampal GABAergic axons. Neuroscience 2005;136:811–822. [PubMed: 16344153]

O'Connor DH, Wittenberg GM, Wang SS. Dissection of bidirectional synaptic plasticity into saturable unidirectional processes. J Neurophysiol 2005;94:1565–1573. [PubMed: 15800079]

Oertel D, Young ED. What's a cerebellar circuit doing in the auditory system? Trends Neurosci 2004;27:104–110. [PubMed: 15102490]

Ohno-Shosaku T, Maejima T, Kano M. Endogenous cannabinoids mediate retrograde signals from depolarized postsynaptic neurons to presynaptic terminals. Neuron 2001;29:729–738. [PubMed: 11301031]

Piomelli D, Beltramo M, Giuffrida A, Stella N. Endogenous cannabinoid signaling. Neurobiol Dis 1998;5:462–473. [PubMed: 9974178]

Pouille F, Scanziani M. Routing of spike series by dynamic circuits in the hippocampus. Nature 2004;429:717–723. [PubMed: 15170216]

Reyes A, Lujan R, Rozov A, Burnashev N, Somogyi P, Sakmann B. Target-cell-specific facilitation and depression in neocortical circuits. Nat Neurosci 1998;1:279–285. [PubMed: 10195160]

Robbe D, Kopf M, Remaury A, Bockaert J, Manzoni OJ. Endogenous cannabinoids mediate long-term synaptic depression in the nucleus accumbens. Proc Natl Acad Sci USA 2002;99:8384–8388. [PubMed: 12060781]

Roberts PD, Bell CC. Computational consequences of temporally asymmetric learning rules: II. Sensory image cancellation. J Comput Neurosci 2000;9:67–83. [PubMed: 10946993]

Rozov A, Burnashev N, Sakmann B, Neher E. Transmitter release modulation by intracellular Ca2+ buffers in facilitating and depressing nerve terminals of pyramidal cells in layer 2/3 of the rat neocortex indicates a target cell-specific difference in presynaptic calcium dynamics. J Physiol 2001;531:807–826. [PubMed: 11251060]

Rubio ME, Juiz JM. Differential distribution of synaptic endings containing glutamate, glycine, and GABA in the rat dorsal cochlear nucleus. J Comp Neurol 2004;477:253–272. [PubMed: 15305363]

Rumsey CC, Abbott LF. Synaptic democracy in active dendrites. J Neurophysiol 2006;96:2307–2318. [PubMed: 16837665]

Safo PK, Regehr WG. Endocannabinoids control the induction of cerebellar LTD. Neuron 2005;48:647–659. [PubMed: 16301180]

Shouval HZ, Bear MF, Cooper LN. A unified model of NMDA receptor-dependent bidirectional synaptic plasticity. Proc Natl Acad Sci USA 2002;99:10831–10836. [PubMed: 12136127]

Sjostrom PJ, Hausser M. A cooperative switch determines the sign of synaptic plasticity in distal dendrites of neocortical pyramidal neurons. Neuron 2006;51:227–238. [PubMed: 16846857]

Sjostrom PJ, Turrigiano GG, Nelson SB. Rate, timing, and cooperativity jointly determine cortical synaptic plasticity. Neuron 2001;32:1149–1164. [PubMed: 11754844]

Sjostrom PJ, Turrigiano GG, Nelson SB. Neocortical LTD via coincident activation of presynaptic NMDA and cannabinoid receptors. Neuron 2003;39:641–654. [PubMed: 12925278]

Sjostrom PJ, Turrigiano GG, Nelson SB. Multiple forms of long-term plasticity at unitary neocortical layer 5 synapses. Neuropharmacology 2007;52:176–184. [PubMed: 16895733]

Sutherland DP, Glendenning KK, Masterton RB. Role of acoustic striae in hearing: discrimination of sound-source elevation. Hear Res 1998;120:86–108. [PubMed: 9667434]

Thomson AM. Activity-dependent properties of synaptic transmission at two classes of connections made by rat neocortical pyramidal axons in vitro. J Physiol 1997;502:131–147. [PubMed: 9234202]

Toth K, Suares G, Lawrence JJ, Philips-Tansey E, McBain CJ. Differential mechanisms of transmission at three types of mossy fiber synapse. J Neurosci 2000;20:8279–8289. [PubMed: 11069934]

Tsien RW, Malinow R. Changes in presynaptic function during long-term potentiation. Ann N Y Acad Sci 1991;635:208–220. [PubMed: 1741585]

Tzounopoulos T, Kim Y, Oertel D, Trussell LO. Cell-specific, spike timing-dependent plasticities in the dorsal cochlear nucleus. Nat Neurosci 2004;7:719–725. [PubMed: 15208632]

Wang SS, Denk W, Hausser M. Coincidence detection in single dendritic spines mediated by calcium release. Nat Neurosci 2000;3:1266–1273. [PubMed: 11100147]

Wang HX, Gerkin RC, Nauen DW, Bi GQ. Coactivation and timing-dependent integration of synaptic potentiation and depression. Nat Neurosci 2005;8:187–193. [PubMed: 15657596]

Wilson RI, Nicoll RA. Endogenous cannabinoids mediate retrograde signalling at hippocampal synapses. Nature 2001;410:588–592. [PubMed: 11279497]

Wilson RI, Nicoll RA. Endocannabinoid signaling in the brain. Science 2002;296:678–682. [PubMed: 11976437]

Wittenberg GM, Wang SS. Malleability of spike-timing-dependent plasticity at the CA3–CA1 synapse. J Neurosci 2006;26:6610–6617. [PubMed: 16775149]

Wouterlood FG, Mugnaini E. Cartwheel neurons of the dorsal cochlear nucleus: a Golgi-electron microscopic study in rat. J Comp Neurol 1984;227:136–157. [PubMed: 6088594]

Yao H, Dan Y. Stimulus timing-dependent plasticity in cortical processing of orientation. Neuron 2001;32:315–323. [PubMed: 11684000]

Yasuda H, Barth AL, Stellwagen D, Malenka RC. A developmental switch in the signaling cascades for LTP induction. Nat Neurosci 2003;6:15–16. [PubMed: 12469130]

Young, ED.; Davis, KA. Circuitry and function of the dorsal cochlear nucleus. In: Oertel, D., et al., editors. Integrative Functions in the Mammalian Auditory Pathway. New York: Springer; 2002. p. 160-206.

Zhang S, Oertel D. Cartwheel and superficial stellate cells of the dorsal cochlear nucleus of mice: intracellular recordings in slices. J Neurophysiol 1993;69:1384–1397. [PubMed: 8389821]

Zucker RS, Regehr WG. Short-term synaptic plasticity. Annu Rev Physiol 2002;64:355–405. [PubMed: 11826273]

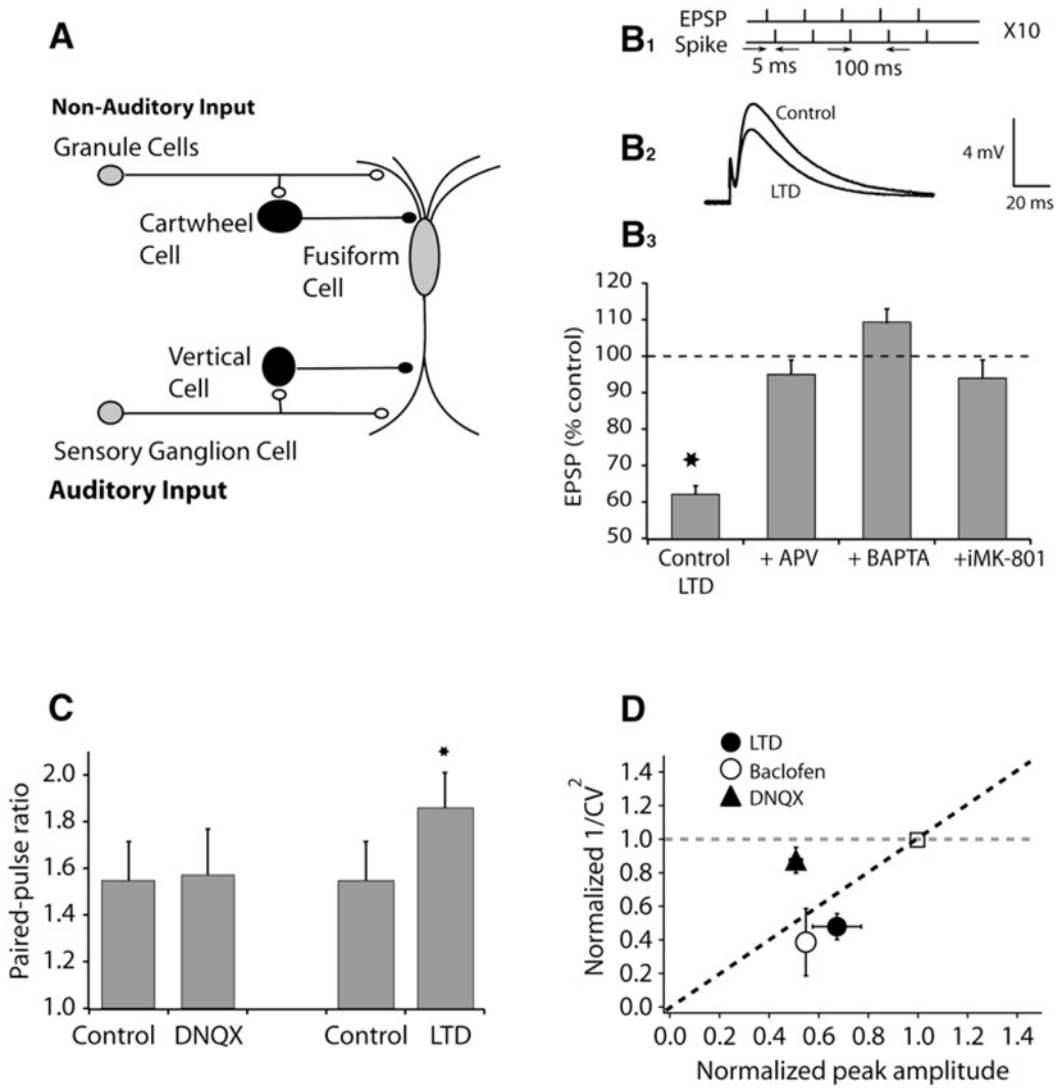

Figure 1. Postsynaptic Induction but Presynaptic Expression Mechanisms Underlie Anti-Hebbian LTD in Cartwheel Cells

(A) Circuitry of the DCN.

(B1) Plasticity was induced by a protocol comprising five pairs (subthreshold EPSP with a current-evoked spike delivered 5 ms later) delivered at 100 ms intervals followed by a 5 s pause, and repeated a total of ten times. (B2) Examples of averaged EPSPs before and 15–20 min after pairing. (B3) Summary graph showing LTD induced by a pairing protocol (control, 62.1% ± 2.3%, n = 8, $p < 0.01$; APV [100 μM], 95% ± 4%, n = 5, ns; BAPTA [20 mM], 109.4% ± 3.6%, n = 6, ns; intracellular MK-801, 94% ± 5%, n = 6, ns).

(C) Paired-pulse facilitation calculated from the ratio of EPSP2/EPSP1 at 50 ms interpulse interval (control, 1.55 ± 0.17, n = 6; DNQX, 1.57 ± 0.20, n = 5, ns; LTD, 1.86 ± 0.15, n = 8, $p < 0.01$).

(D) $1/CV^2$ analysis; partial block of postsynaptic AMPA receptors by 0.5 μM DNQX and presynaptic inhibition induced by GABA-B agonist baclofen (2–5 μM) verify that CV analysis can identify locus of suppression. CV analysis suggests that LTD is expressed presynaptically. All means are reported ± SEM.

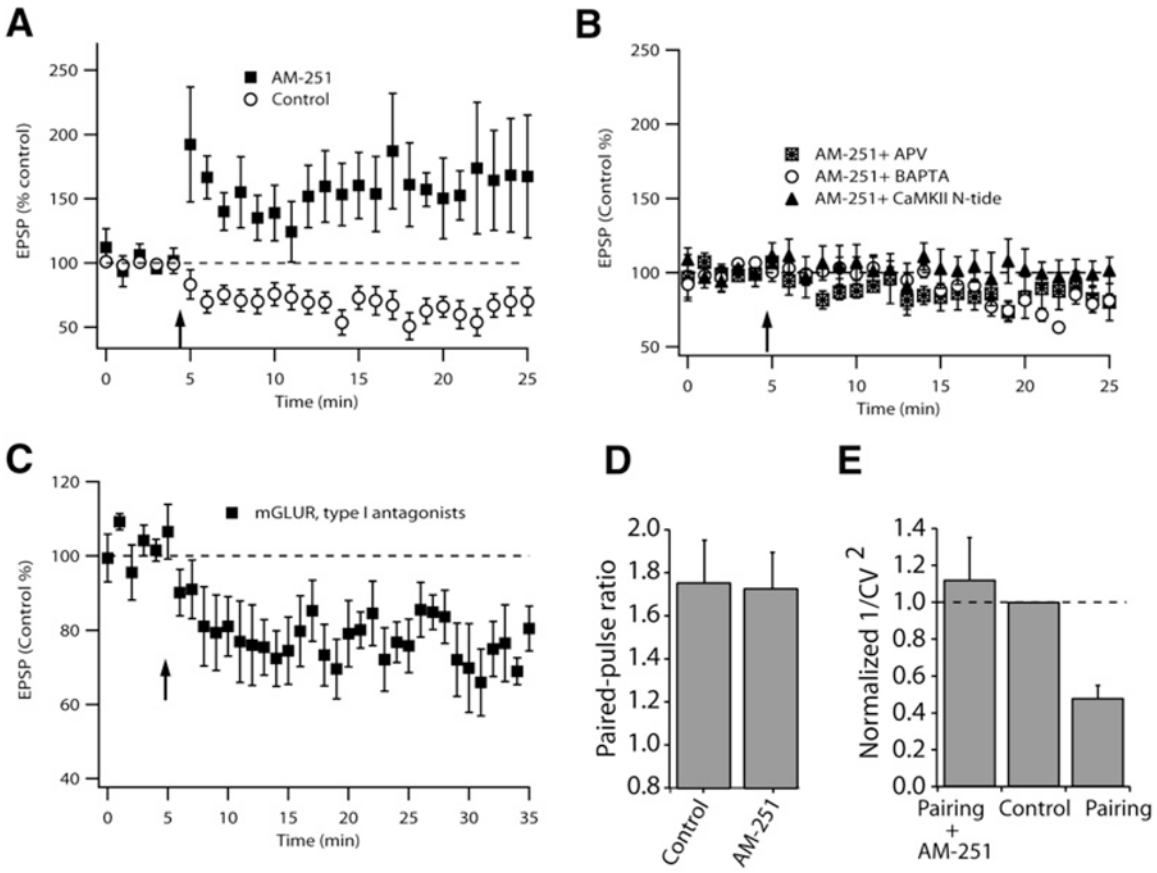

Figure 2. Role of Endocannabinoid and CaMKII in Synaptic Plasticity in Cartwheel Cells

(A) Time course of induced plasticity (control, LTD, 62% ± 2%, n = 8; AM-251, LTP, 163% ± 10%, n = 7).

(B) Failure to induce plasticity in the presence of AM-251 plus APV (86% ± 5%, n = 5, ns); BAPTA (80% ± 6%, n = 5, ns); CaMKII-Ntide (100% ± 5%, n = 6, ns).

(C) LTD was induced in the presence of 100 μM LY367385 and 4 μM MPEP, selective antagonists of mGluR subtypes 1 and 5, respectively. The magnitude of LTD was not significantly different from control LTD (74% ± 2.5%, n = 6).

(D) Paired-pulse facilitation (control, 1.75 ± 0.2, n = 7; AM-251, 1.72 ± 0.2, n = 6). Control values are from the same cells but before the pairing protocol was initiated.

(E) $1/CV^2$ analysis of cartwheel cell, suggesting that LTP is expressed postsynaptically while LTD is expressed presynaptically (AM-251 + pairing, normalized $1/CV^2 = 1.12 \pm 0.2$ of control, n = 5, ns; pairing alone, normalized $1/CV^2 = 0.48 \pm 0.1$, n = 6, $p < 0.05$).

All experiments used the 5 ms pre-post interval as in Figure 1. All means are reported ± SEM.

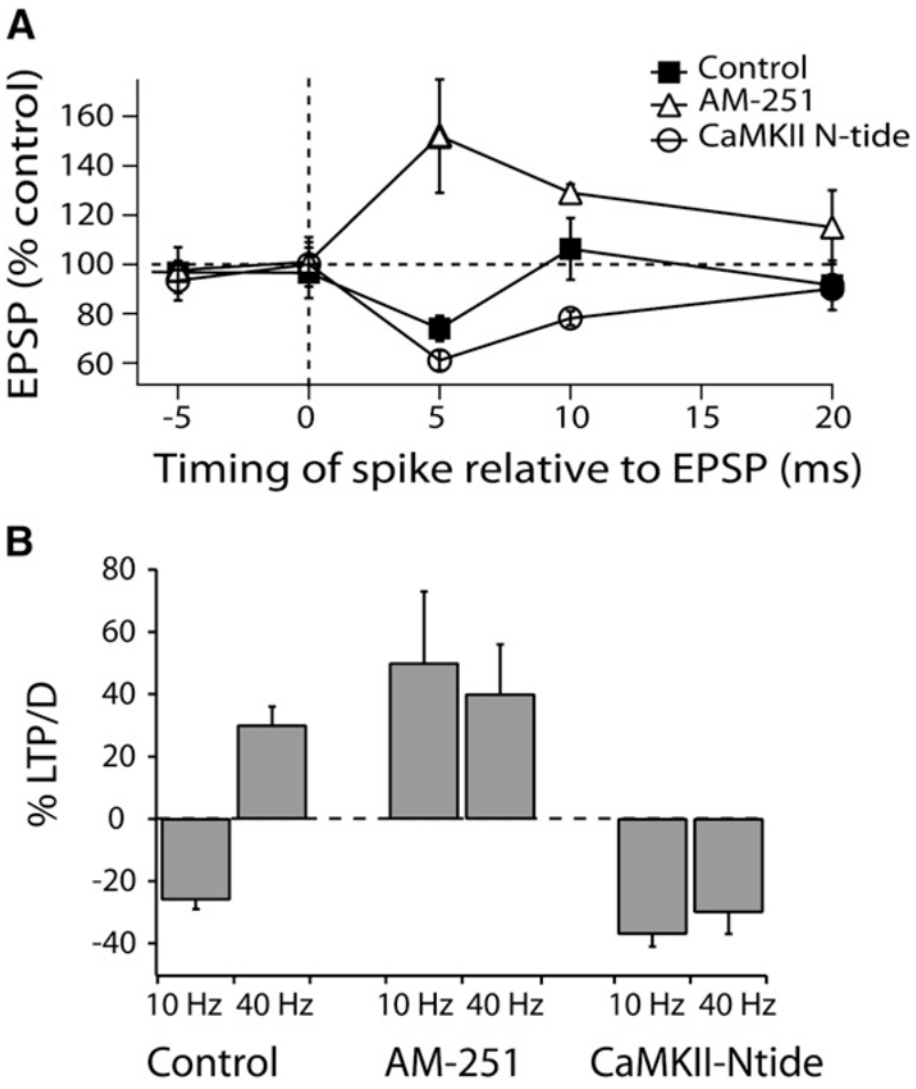

Figure 3. Synaptic Learning Rules Determined by Interaction of Distinct Signaling Mechanisms and Levels of Synaptic Activity

(A) Synaptic timing plot for cartwheel cells when pairs (EPSP followed or preceded by a current-evoked spike delivered within 20 ms) were delivered at 100 ms intervals (10 Hz). Time points are shown as the average interval between EPSP onset and spike peak measured in each experiment. Data are means from 4 to 13 cells per point.

(B) Frequency dependence of STDP observed with EPSP spike sequence at 5 ms interval, and pairs delivered at either 10 and 40 Hz (control 10 Hz, −25% ± 5%, n = 8, control 40 Hz, +30% ± 6%, n = 6; AM-251 10 Hz, +50% ± 23%, n = 5, AM-251 40 Hz, +40% ± 16%, n = 5; CaMKII-Ntide 10 Hz, −37% ± 4%, n = 5, CaMKII-Ntide 40 Hz, −30% ± 7%, n = 6).

All means are reported ± SEM.

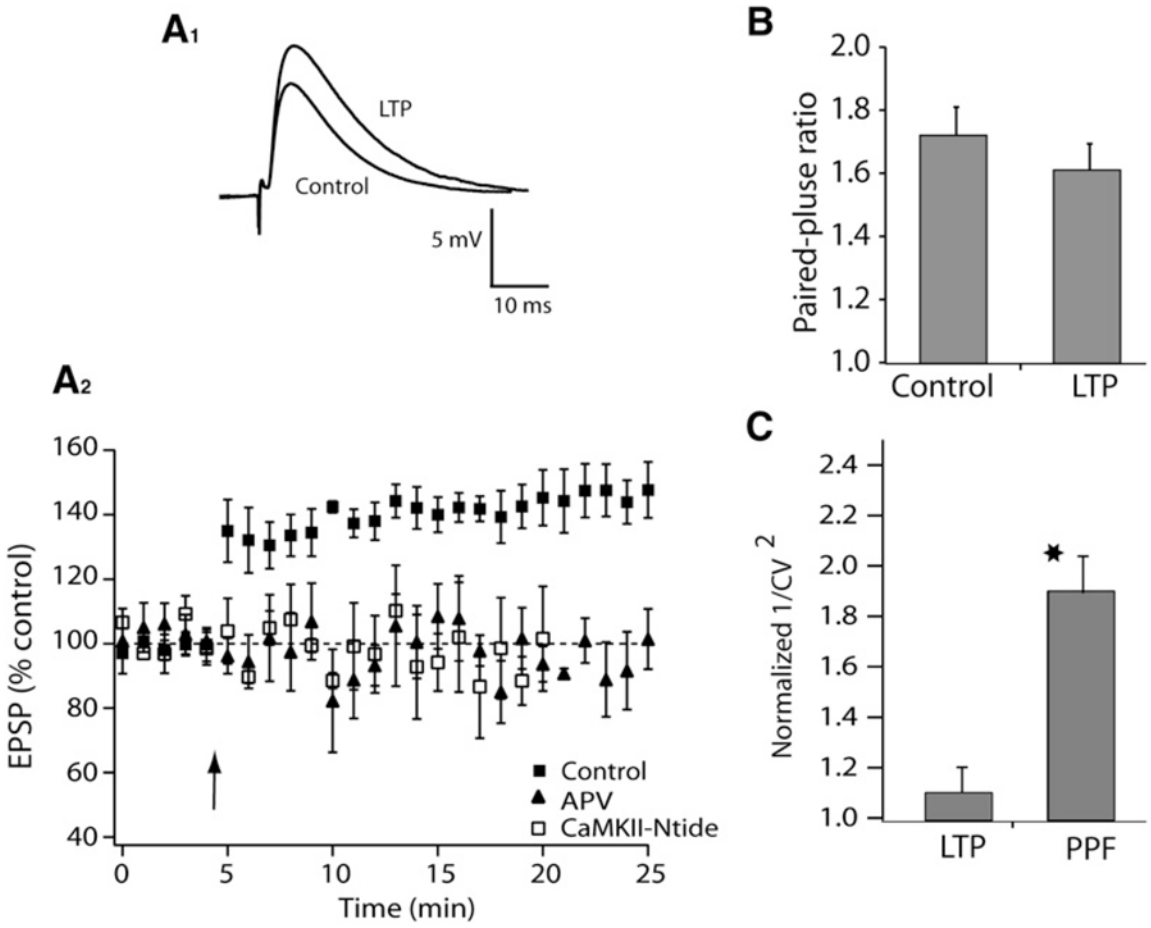

Figure 4. Postsynaptic Induction and Expression Mechanisms Underlie LTP in Fusiform Cells

Plasticity was induced by a protocol comprising five pairs (subthreshold EPSP with a current-evoked spike delivered 5 ms later) delivered at 100 ms intervals followed by a 5 s pause, and repeated a total of ten times.

(A1) Examples of averaged EPSPs before and 15–20 min after pairing. (A2) Time course of induced plasticity in fusiform cells (control, 146% ± 7%, n = 8, $p < 0.05$; APV, 95% ± 2%, n = 6, ns; CaMKII-Ntide, 95% ± 3%, n = 6, ns).

(B) Summary graph showing paired-pulse facilitation (PPF) (control, 1.72 ± 0.09, n = 6; LTP, 1.61 ± 0.08, n = 7).

(C) $1/CV^2$ analysis: LTP 1.1 ± 0.1, n = 8; PPF: 1.9 ± 0.2, n = 7. Values for EPSP potentiation with LTP (measured after 15–20 min) and PPF: 1.35 ± 0.01 and 1.43 ± 0.01, respectively. All means are reported ± SEM.

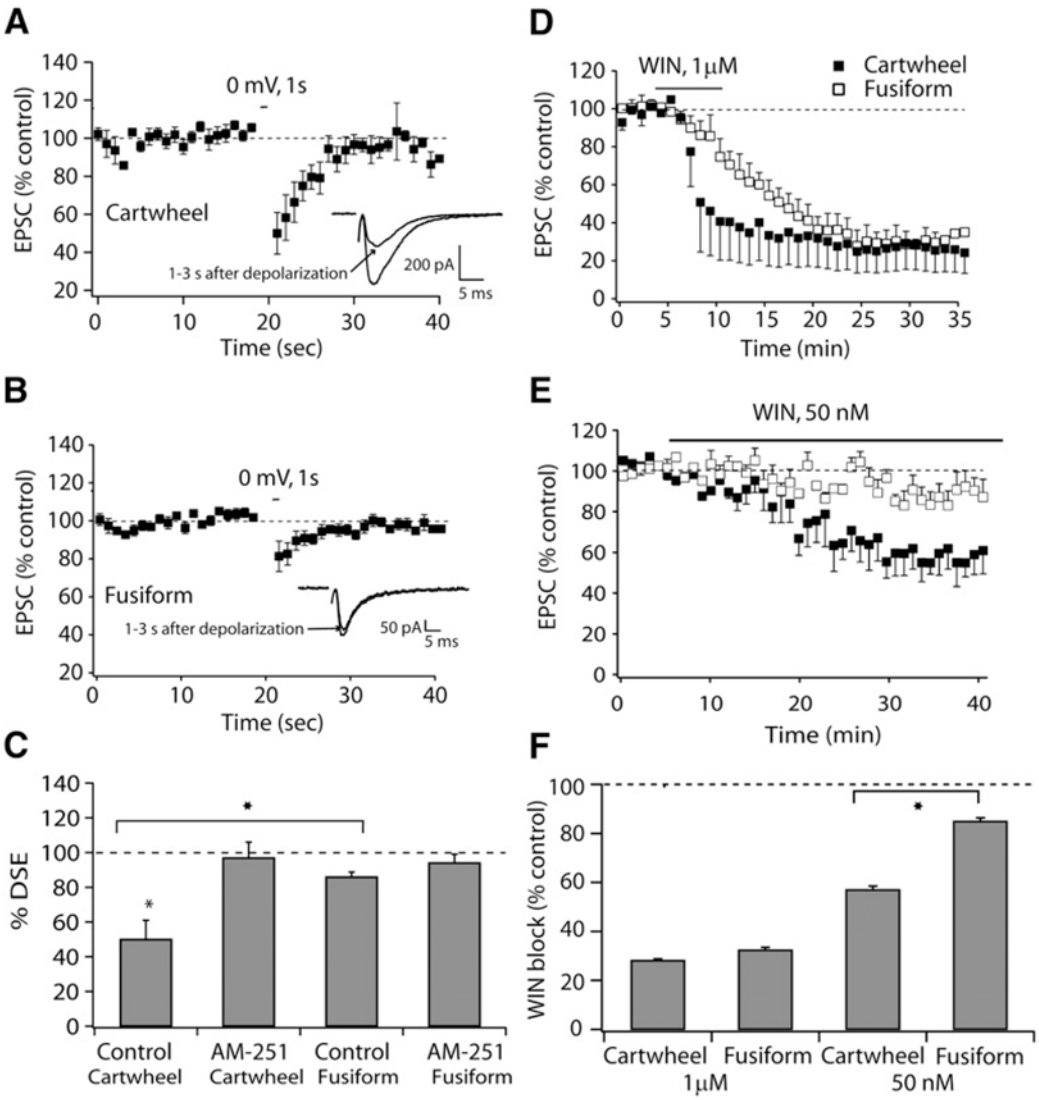

Figure 5. Differential Engagement of Endocannabinoid Signaling in Cartwheel and Fusiform Cells

(A) Time course of DSE, induced by 1 s depolarization in cartwheel cells, inset showing EPSCs before and after depolarization to 0 mV.

(B) Time course of DSE, induced by 1 s depolarization in fusiform cells, inset showing EPSCs before and after depolarization to 0 mV.

(C) Pharmacology and comparison of average DSE in cartwheel and fusiform cells. (EPSC before/EPSC 1 s after depolarization is terminated) × 100 (cartwheel cells: control, 50% ± 11%, n = 9; 1 μM, bath-applied AM-251, 97% ± 9%, n = 7; fusiform cells: control, 86% ± 3%, n = 8, 1 μM, bath-applied AM-251, 94% ± 5%, n = 5).

(D) Time course of 1 μM WIN block of transmission in cartwheel and fusiform cells.

(E) Time course of 50 nM WIN block of transmission in cartwheel and fusiform cells.

(F) Summary graph showing comparison of average WIN block (EPSC before/EPSC 25–30 min after application of WIN) between fusiform and cartwheel cells (1 μM WIN: cartwheel cells 28% ± 6%, n = 4; fusiform cells, 32% ± 1%, n = 4, 50 nM WIN: cartwheel cells 57% ± 1%, n = 4; fusiform cells 85% ± 1%, n = 4).

All means are reported ± SEM.

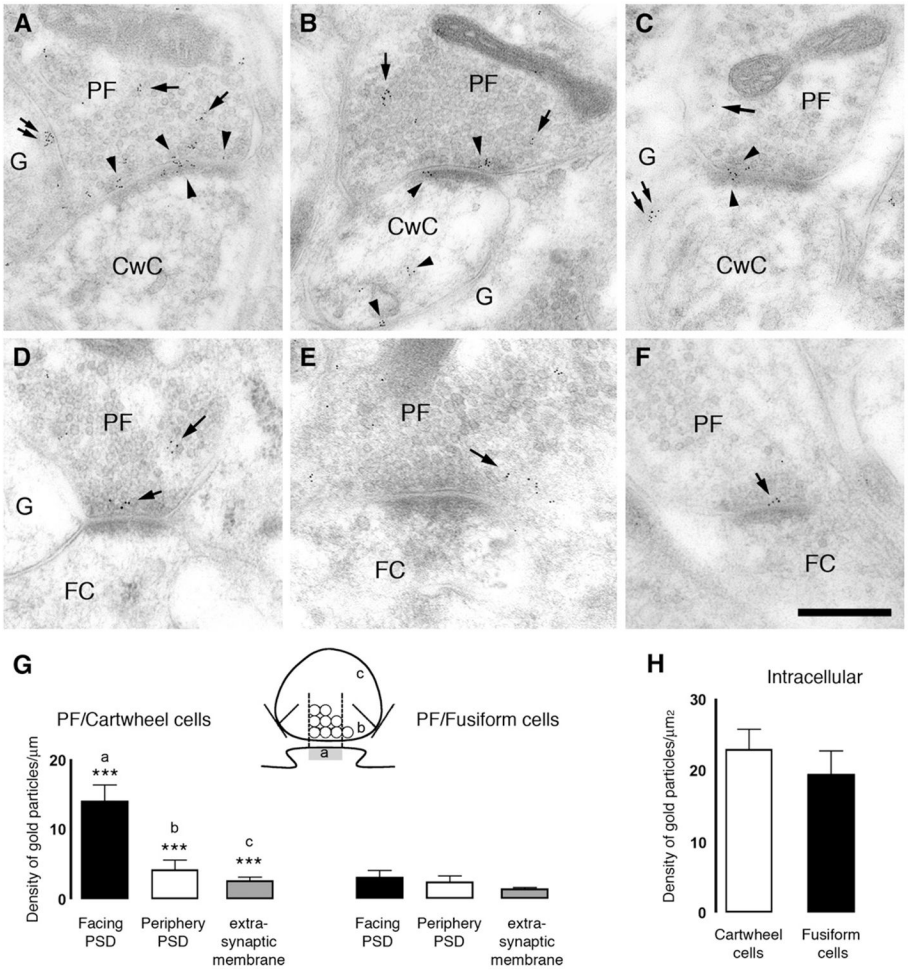

Figure 6. CB1 Receptors Are Differentially Expressed at Parallel Fiber Synapses in DCN

Electronmicrographs show postembedding immunogold labeling using the CT antibody for CB1 receptor at the parallel fiber (PF)/cartwheel cell (CwC) (A–C) and parallel fiber/fusiform cell (FC) (D–F) synapses. Gold particles for CB1 were observed at the presynaptic boutons (arrows) of parallel fibers synapsing on apical dendrites of FC. Three patterns of immunogold labeling were observed: (1) gold particles associated with the presynaptic membrane, (2) gold particles associated with plasma membrane not facing synapses or extrasynaptic plasma membrane, and (3) gold particles associated with synaptic vesicles intracellularly. In the dendritic spines of cartwheel cells but not fusiform cells gold particles were observed associated with intracellular compartments or plasma membrane (arrowheads). Glial cells (G) also presented gold particles for CB1 (double arrows in [A] and [C]). Scale bar, 0.25 μm. (G) Density of gold particles/mm length ± SEM for CB1 of the parallel fiber synaptic ending plasma membrane. The plasma membrane of the parallel fiber synaptic terminal was divided into three regions, illustrated in the cartoon: parallel fiber membrane facing the PSD (*a*); parallel fiber membrane facing the periphery of the PSD (*b*); and parallel fiber membrane not facing the synapse (*c*) on cartwheel and fusiform cells (***$p < 0.001$). (H) Density of gold particles/ μm^2 area ± SEM of the intracellular pool of CB1 in the parallel synaptic terminal onto cartwheel and fusiform cells.